

THERMAL AND CHEMICAL EQUILIBRATION
IN A GLUON PLASMA

S.M.H. Wong

¹*LPTHE, Université de Paris XI, Bâtiment 211,
F-91405 Orsay, France*

Abstract

We show the evolution of a gluon plasma towards equilibrium starting at some early moment when the momentum distribution in the central region is momentarily isotropic. Using HIJING results for Au+Au collision as initial input, we consider thermalization and chemical equilibration simultaneously at both LHC and RHIC energies. Thermalization is shown to be driven chiefly by inelastic process in our scenario contradicting common assumption that this is the role of elastic process. We argue that only the inelastic dominance depends on the initial conditions but not the dominance itself.

LPTHE-Orsay 96/07

¹Laboratoire associé au Centre National de la Recherche Scientifique

1 Introduction

In future heavy ion collision experiments at the Relativistic Heavy Ion Collider (RHIC) at Brookhaven and at the Large Hadron Collider (LHC) at CERN, one hopes to create a new state of matter, the quark-gluon plasma. In order to clearly distinguish this from the possible alternative of a hadron gas, one would like to know the state of the plasma in its different stages throughout its lifetime. With this knowledge, the conditions under which different possible signatures of the plasma are produced and the time at which they are produced can be compared with those of the hadron gas [1]. It is precisely the difference of these conditions and the time dependence which could permit a possible distinction from a hadron gas and a clear identification of a quark-gluon plasma. There have already been numerous works in the direction of the possible signatures and also a number of investigations on the various time scales and stages of the plasma. In this work, we will focus on the latter.

In the following, we will not attempt to match the comprehensiveness and details of the semi-classical parton cascade model [2, 3] which models the evolution in relativistic heavy ion collisions by tracing the phase space history of the particles and combining perturbative QCD with relativistic transport theory. Our approach will base on rather simple assumptions and initial conditions which have already been made used of in the previous studies of thermalization and parton chemical equilibration [4, 5, 6, 7].

In many previous studies [1, 4, 5, 6, 8, 9] of relativistic heavy ion collisions, a convenient assumption and starting point is kinetic equilibration is very rapid ≤ 1 fm and hydrodynamic expansion is well underway. As has been pointed out in [7, 10], collisions are not sufficiently rapid at early times to maintain thermal equilibrium in an expanding plasma, so the system is more likely to be in a situation between free streaming, where there is no collision or the collision effects are completely negligible, and hydrodynamic expansion when local kinetic equilibrium has been achieved. Various studies have been made in determining the relation between collision time θ and the degree of equilibration of the plasma [7, 11, 12] based on relaxation time approximation and assumed simple power behaviour of $\theta \sim \tau^p$. In this work, we will also look at the collision time and thermalization but we do not assume a priori any form for θ , rather it will be determined entirely from the interactions. Our starting point will be different from many previous works in that we start somewhere between free streaming and hydrodynamic expansion. Some initial steps in this direction have been taken by Heiselberg and Wang in [7] but they only considered elastic interactions and only in the time range $\tau_0 \lesssim \tau \ll \theta$, where τ_0 is the initial time which will be further explained below. Following their initial line of approach, we attempt to give a more complete treatment. We will do this under certain assumptions and approximations which will be explained in the subsequent sections. The method that will be shown here allows the treatment of the out of equilibrium plasma with comparative ease. We will illustrate this approach by applying it to the simpler case of a pure gluon plasma. Thermal as well as chemical equilibration of the gluon plasma will be investigated. That of a quark-gluon plasma will be dealt with in a

subsequent paper [13].

For the initial conditions, we will use results obtained from the Monte Carlo HIJING model [14, 15, 16] as have been used in [4] and later improved in [5, 6] but we will interpret them in a slightly different way so that our initial temperatures T_0 and fugacities l_0 are not the same as theirs although we use the same initial gluon energy densities ϵ_0 and number densities n_0 .

In principle, one could vary the initial conditions and look at the resulting evolution of the plasma as have been done in [8] since HIJING predictions for the energy densities and number densities are in the low end in comparison with, for example, those from the parton cascade model [3] but we will not do that here. We would rather concentrate on one set of specific initial conditions each at RHIC and LHC energies and look at the thermalization, isotropy of momentum distribution and the time dependence of fugacity, collision time θ and a modified form of the non-equilibrium colour screening length. We show, in particular, inelastic process dominates over the elastic one in the approach towards equilibrium and this is independent of initial conditions. The degree of this dominance, however, is dependent on initial conditions.

The paper is organized as follows. In Sect. 2, the various assumptions, approximations and approach will be described. Sect. 3 is devoted to calculating rates for the interactions that we will consider and the set of equations to use for chemical equilibration will be given. Initial conditions used and the method of computation will be outlined in Sect. 4. Lastly, the results of the evolution of the gluon plasma will be shown and discussed in Sect. 5.

2 Boltzmann Equation and Relaxation Time Approximation

In a many-body system, it is expedient to use particle distributions $f(\mathbf{p}, \mathbf{r}, \tau)$ as well as collective variables energy density ϵ , number density n , entropy density s etc. or at least local collective variables to describe the spatial as well as temporal variation of the system. This is what we will do here but we concentrate mainly in the central collision region which we assume to be essentially uniform in space. Ideally, one would like to describe $f(\mathbf{p}, \tau)$ by a set of fully relativistic and quantum transport equations derived from first principle of QCD [17, 18] since a quark-gluon plasma is inherently a quantum system. But unfortunately, this has not yet been realized although various advances have been made in that direction based on constructing Wigner operators from the fields and deriving their equations of motion from the field equations [19, 20]. The difficulty is partly due to the complexity of the equations of motion for the Wigner operators which requires, in the end, one to make a semi-classical expansion in powers of \hbar and partly due to the gauge degrees of freedom which make it hard to identify a gluon distribution operator [21]. These gauge degrees of freedom of QCD have proved to be

a stumbling block in identifying a Wigner operator as the gluon distribution operators. Recent works [22, 23] suggest that this latter problem could be overcome by choosing the radial gauge but one has yet to derive the collision terms.

Under these circumstances, one has to make do with relativistic but semi-classical approach such as using Boltzmann equation

$$\left(\frac{\partial}{\partial t} + \mathbf{v} \cdot \frac{\partial}{\partial \mathbf{r}}\right) f(\mathbf{p}, \mathbf{r}, t) = C(\mathbf{p}, \mathbf{r}, t), \quad (1)$$

and combining it with collision term C obtained from QCD. Assuming one-dimensional expansion along the z -axis [24] and boost invariance or rapidity independence of the central region, Baym [11] showed that Eq. (1) can be rewritten as

$$\left(\frac{\partial f(p_{\perp}, p_z, \tau)}{\partial \tau}\right)\Big|_{p_z \tau} = C(p_{\perp}, p_z, \tau). \quad (2)$$

As in [7, 11], we use the relaxation time approximation for the collision term

$$C(\mathbf{p}, \tau) = -\frac{f(\mathbf{p}, \tau) - f_{eq}(\mathbf{p}, \tau)}{\theta(\tau)} \quad (3)$$

which enables us to write down a solution to the Boltzmann equation Eq. (2)

$$f = f_0(p_{\perp}, p_z \tau / \tau_0) e^{-x} + \int_0^x dx' e^{x'-x} f_{eq}(\sqrt{p_{\perp}^2 + (p_z \tau / \tau')^2}, T_{eq}(\tau')), \quad (4)$$

where

$$x(\tau) = \int_{\tau_0}^{\tau} d\tau' / \theta(\tau'), \quad (5)$$

given some initial distribution f_0 at τ_0 . $f_0(p, \tau)$ is the free streaming, $C = 0$, solution to Eq. (2). Our solution differs from that in [7]. In their case, they considered only elastic interactions and so had to keep a chemical potential $\mu(\tau')$ in f_{eq} . We will not restrict ourselves to only these interactions. On the contrary, we will use the interaction $gg \longleftrightarrow ggg$ to determine $\theta(\tau)$. $T_{eq}(\tau)$ in f_{eq} is determined from energy conservation

$$\epsilon(\tau) = \epsilon_{eq}(\tau) = a_2 T_{eq}^4(\tau), \quad (6)$$

with $a_2 = 8\pi^2/15$. It is the momentaneous target temperature that the gluon plasma is striving to reach. The associated energy conservation equation is [11]

$$\frac{d\epsilon}{d\tau} + \frac{\epsilon + p_L}{\tau} = 0, \quad (7)$$

and p_L is the longitudinal pressure in the z -direction given by

$$p_L(\tau) = \nu \int \frac{d^3 \mathbf{p}}{(2\pi)^3} \frac{p_z^2}{p} f(p_{\perp}, p_z, \tau), \quad (8)$$

with $\nu = 2 \times 8 = 16$ for the multiplicity of gluons. Along the same line, we can also defined p_T , the transverse pressure by replacing p_z by p_x or p_y in Eq. (8). These pressures will be used to check the degree of anisotropy of momentum distribution in the central region of the plasma.

3 Rate Equations

To consider chemical equilibration, we require the rate equations for gluon creation or destruction. From [25] and Eq. (2), we have the following rate equation for the gluon number density

$$\frac{\partial n}{\partial \tau} + \frac{n}{\tau} = \sigma \int \frac{d^3 \mathbf{p}}{(2\pi)^3} C(\mathbf{p}, \tau) = R(\tau) , \quad (9)$$

and using Eq. (2) and Eq. (3), we also have

$$R(\tau) = \frac{n_{eq}(\tau) - n(\tau)}{\theta(\tau)} , \quad (10)$$

where $n_{eq}(\tau) = a_1 T_{eq}^3(\tau)$ and $a_1 = 16\zeta(3)/\pi^2$. The σ in Eq. (9) is a numerical factor to take into account of multiplicity and symmetry of the permutations of the gluons in C . The two equations Eq. (9) and Eq. (10) allow us to determined $\theta(\tau)$ at any instance in time.

For the r.h.s. of Eq. (9), we take this to be the simplest gluon multiplication process $gg \longleftrightarrow ggg$

$$\begin{aligned} \sigma \int \frac{d^3 \mathbf{p}}{(2\pi)^3} C(\mathbf{p}, \tau) &= \frac{1}{4} (2\pi)^4 \nu^2 \prod_{i=1}^5 \frac{d^3 \mathbf{p}_i}{(2\pi)^3 2p_i} |\mathcal{M}_{gg \rightarrow ggg}|^2 \delta^4(p_1 + p_2 - p_3 - p_4 - p_5) \\ &\quad \times [f_1 f_2 (1 + f_3)(1 + f_4)(1 + f_5) - f_3 f_4 f_5 (1 + f_1)(1 + f_2)] \\ &\quad \times \theta(\Lambda - \tau_{QCD}) . \end{aligned} \quad (11)$$

The various parts of this formula need some explanation, we do this one by one. Here we only consider small angle scattering and without loss of generality p_5 is taken to be a soft gluon radiation around zero rapidity in the centre of momentum frame so that we can use Bertsch and Gunion formula [26] for the amplitude. In that frame of the two incident gluons, where they approach each other on the z-axis, this is

$$|\mathcal{M}_{gg \rightarrow ggg}|^2 = \left(\frac{4g^4 N^2}{N^2 - 1} \frac{s^2}{(\mathbf{q}_\perp^2 + m_D^2)^2} \right) \left(\frac{4g^2 N \mathbf{q}_\perp^2}{\mathbf{k}_\perp^2 [(\mathbf{k}_\perp - \mathbf{q}_\perp)^2 + m_D^2]} \right) \quad (12)$$

where \mathbf{k}_\perp and \mathbf{q}_\perp are the perpendicular component of \mathbf{p}_5 and that of the momentum transfer in that frame respectively. $N = 3$ is for SU(3) of QCD and s is the total centre of mass energy. The first part on the r.h.s. within round brackets is the squared modulus of the small angle elastic scattering amplitude for $gg \rightarrow gg$ and the second part is essentially the soft gluon emission spectrum. Since the centre of momentum frame of any two incident gluons are very unlikely to be the same as the plasma rest frame, we need a general formula for this amplitude. In the plasma rest frame, one simply substitutes

$$(\mathbf{k}_\perp - \mathbf{q}_\perp)^2 = 4 p_1 \cdot p_3 p_2 \cdot p_3 / s \quad (13)$$

$$\mathbf{q}_\perp^2 = 4 p_1 \cdot p_4 p_2 \cdot p_4 / s \quad (14)$$

$$\mathbf{k}_\perp^2 = 4 p_1 \cdot p_5 p_2 \cdot p_5 / s \quad (15)$$

in Eq. (12).

We have infrared regularized the squared modulus of the amplitude Eq. (12) with the Debye screening mass m_D^2 which is time dependent in the present case. We take it to be defined at leading order in α_s by

$$m_D^2(\tau) = -8\pi\alpha_s N \int \frac{d^3\mathbf{p}}{(2\pi)^3} \frac{\partial f(\mathbf{p}, \tau)}{\partial |\mathbf{p}|}. \quad (16)$$

Note that the screening mass should be directional dependent in general [27, 28] but rather than keeping tracks of the directions of the gluons, we simplified this by removing the directional dependence. The present form can be thought of as an averaged screening mass between the transverse and longitudinal screening. We will explain this in some details elsewhere [13]. Here f is not of the Bose-Einstein form when the plasma is out of equilibrium but is given by Eq. (4). It reduces, of course, to the familiar $m_D^2 = 4\pi\alpha_s T^2$ when in equilibrium. This provides us with a general Debye screening mass to screen off infrared divergences even in out of equilibrium situation which is the subject of this paper.

As in [4, 5, 6], we use the approach of Gyulassy and Wang [29, 30] to deal with the Landau-Pomeranchuk-Migdal (LPM) suppression of soft gluon radiations due to multiple scattering of the parent gluon in a medium. This is taken into account in the form of the θ -function in Eq. (11). The basis of this approach is to include only the non-suppressed Bethe-Heitler limit but the suppressed emission between that and the factorization limit is completely dropped. Ideally, one would also like to include these emissions. The θ -function requires that the mean free path, Λ , of the gluon which we take from the small angle gg elastic scattering cross-section [4, 5, 6],

$$\frac{d\sigma_{el}^{gg \rightarrow gg}}{d\mathbf{q}_\perp^2} = \frac{9}{4} \frac{2\pi\alpha_s^2}{(\mathbf{q}_\perp^2 + m_D^2)^2} \quad (17)$$

$$\Lambda^{-1} = n \int_0^{s/4} d\mathbf{q}_\perp^2 \frac{d\sigma_{el}^{gg \rightarrow gg}}{d\mathbf{q}_\perp^2} = \frac{9\pi\alpha_s^2 sn}{8m_D^2(s/4 + m_D^2)} \quad (18)$$

to be larger than the formation time $\tau_{QCD} = k_0/\mathbf{k}_\perp^2$ of the soft gluon. This LPM effect on the radiative energy loss of a fast energetic parton previously derived in [30] has been improved and rederived recently in [31] by including interference graphs where the emitted gluon also undergoes multiple scattering with the scattering centres. However, the derived soft radiation LPM spectrum has no dependence on the direction of the emitted gluon. This has to be integrated out for the radiation density to make sense. As such, their result cannot be used in the present problem. One will have to be contented to include only the Bethe-Heitler non-suppressed emission therefore we use the same θ function as in [4, 5, 6].

At this point, a remark is in order concerning large angle scattering non-soft gluon emission. In [8], Shuryak and Xiong found that large angle scattering is also important

and higher order tree diagrams of maximal helicity violating amplitudes, the so called Kunszt-Stirling [32] corrected Park-Taylor formula [33] for gluon multiplication are not negligible. In performing their calculation, LPM suppression has been totally neglected. As far as the author is aware, possible interference effect on non-soft gluon emission in multiple scattering has not been worked out. May be this is negligible for non-soft radiation if one is permitted to generalize the language of the soft emission to the non-soft case. That is by arguing that the gluon mean free path is approximately the same or larger than the coherence length of these radiations, but the latter is not defined for non-soft radiation. Facing the choice of giving up LPM entirely or including large angle scatterings, we choose the first alternative. The latter will be investigated in a future work where some form of LPM or more general interference effect due to multiple scattering will have to be included.

4 Initial Conditions for the Computations

As in [4, 5, 6, 7], we consider the following scenario. Initially, the two incoming heavy ions which have been accelerated to very high energies, 200 GeV/nucleon at RHIC and up to 6.3 TeV/nucleon at LHC, along the z-axis collide, penetrate each other leaving behind in the central region a gas of secondary partons produced via minijets [34]. Since most energies are in the longitudinal direction, the momentum distribution is mainly along the beam direction. As mentioned in the introduction, collision time is larger than the expansion time so initially the partons are more likely to stream freely in the longitudinal direction gradually suppressing the momentum distribution in that direction in the central region. One can understand this by looking at the form of f_0 in Eq. (22). At certain moment τ_0 , longitudinal momentum distribution will be reduced to such an extent that it becomes the same as the transverse momentum distribution, or in other words, the momentum distribution becomes isotropic. Assuming a thermal distribution at this time τ_0 fixes $f_0(\mathbf{p}, \tau_0)$. The initial temperature T_0 and fugacity l_0 can be determined from the gluon energy density and number density. These values will be taken from the improved version [5] of [4] but we obtain the temperature and fugacity in a slightly different way. In [4, 5], they used the fugacity factorized thermal equilibrium form of f , i.e.

$$f(\mathbf{p}, l) = \frac{l}{\exp(|\mathbf{p}|/T) - 1} \quad (19)$$

for all values of l . As was pointed out in their work, this is a good approximation only when $l \approx 1$. Here we keep the original form of f at least whenever it is in thermal equilibrium. We get the initial temperature T_0 and fugacity l_0 at τ_0 by observing that l_0 is small initially, at least in HIJING results, when we can approximate f by the Boltzmann form $f = l e^{-p/T}$ so the energy density ϵ_0 and number density n_0 are given by

$$\epsilon_0 = 3 \nu l_0 T_0^4 / \pi^2 \quad \text{and} \quad n_0 = \nu l_0 T_0^3 / \pi^2, \quad (20)$$

respectively. The extracted T_0 and l_0 for Au+Au collision at LHC and at RHIC are shown in Table 1. Knowing

$$f_0(\mathbf{p}, \tau_0) = \frac{l_0}{\exp(|\mathbf{p}|/T_0) - l_0}, \quad (21)$$

we can deduce the time dependent form for it, since it is the free streaming solution to Eq. (2) [7, 11]

$$f_0(p_\perp, p_z, \tau) = \frac{l_0}{\exp(\sqrt{p_\perp^2 + p_z^2 \tau^2 / \tau_0^2} / T_0) - l_0}. \quad (22)$$

Using this, we can calculate the rate $gg \longleftrightarrow ggg$ at τ_0 and hence θ_0 . With these initial values, we start the evolution of the plasma.

The evolution of the gluon plasma is performed as follows. Phase space integrals for calculating the gluon multiplication rate are performed by an iterative and adaptive Monte Carlo method VEGAS [35]. All time integrals are calculated by discretizing time τ so that any function $G(\tau)$ depending on a time integral of another function $g(\tau, \tau')$ is re-expressed as

$$G(\tau) = \int_{\tau_0}^{\tau} d\tau' g(\tau, \tau') \implies G(\tau_n) \approx \sum_{i=0}^{n-1} \Delta\tau g(\tau_n, \tau_i), \quad (23)$$

where $\tau_i = \tau_0 + i\Delta\tau$ and $\Delta\tau$ is some small chosen time step. Then $G(\tau_n)$ is determined entirely by variables of the preceding time steps from τ_0 to τ_{n-1} . Given all the variables at t_0 , the same set of variables at τ_1 can be determined. This procedure is repeated for obtaining the variables at τ_2 from those at τ_0 and τ_1 and so on. The set of variables to determine are $\epsilon(\tau)$ for obtaining $T_{eq}(\tau)$ which enables the determination of $m_D^2(\tau)$. This modified screening mass is required for calculating $R(\tau)$ which together with $n(\tau)$ and $T_{eq}(\tau)$ allow us to obtain $\theta(\tau)$. Both $\theta(\tau)$ and $T_{eq}(\tau)$ are essential for finding $f(\mathbf{p}, \tau)$ which is itself needed in $R(\tau)$ and for the calculations of the various collective variables.

5 Equilibration of the Gluon Plasma

The results of the evolution towards equilibrium of a gluon plasma for two sets of initial conditions for Au+Au collisions at LHC and at RHIC are presented in Fig. 1, 2 (LHC) and Fig. 3, 4 (RHIC). These are results calculated using $\alpha_s = 0.3$ and $\Delta\tau = 0.05$ fm/c. Using smaller values of $\Delta\tau$, for example, $\Delta\tau = 0.02$ fm/c shifts the various values by amounts ranging up to 6.25%. Since we are not going after high numerical accuracy, we will settle for the present value. In any case, there is no qualitative change by varying $\Delta\tau$. Unless explicitly stated otherwise, the dashed curves in most figures are the equilibrium values associated with f_{eq} in Eq. (3). The solid curves are the actual results. One sees that the two curves approach each other with increasing time. How close the solid and dashed curves are is a measure of how close the plasma is to

equilibrium. The computation is stopped when the estimated temperature falls below 200 MeV. This and the fugacity are estimated by using the expression for the near full equilibrium energy and number density

$$\epsilon = a_2 l T^4 \quad \text{and} \quad n = a_1 l T^3 \quad (24)$$

which are valid when l is close to one, so that

$$T_{est} = a_1 \epsilon / (a_2 n) \quad \text{and} \quad l_{est} = a_2^3 n^4 / (a_1^4 \epsilon^3) . \quad (25)$$

Since we have used energy conservation $\epsilon(\tau) = \epsilon_{eq}(\tau)$ at all time so in Fig. 1 and 3 (a) where we show the evolution of the energy densities, the solid and dashed curves coincide. Comparing gluon densities in Fig. 1 and 3 (b), the estimated temperatures in Fig. 1 and 3 (c), the entropy densities in Fig. 1 and 3 (e) and the squared of the modified screening mass in Fig. 2 and 4 (b), it is apparent that at LHC, the solid and dashed curves are much closer to each other at the end of the calculation than they are at RHIC. Those at LHC are actually lying on top of each other or at least very close. The estimated fugacity l_{est} at the end of the calculation is about 0.94 at LHC and 0.40 at RHIC. The time evolution of these and the estimated temperatures are shown in Fig. 1 and 3 (c). The dot-dashed curves are the fugacity evolutions. Note that these estimated values can only be viewed as indicators. It will be seen that the plasma have not quite completely thermalized at the end of the calculations.

The entropy density evolutions $s(\tau)$ shown in Fig. 1 (e) for LHC and in Fig. 3 (e) for RHIC are calculated from [36]

$$s(\tau) = -\nu \int \frac{d^3 \mathbf{p}}{(2\pi)^3} \left\{ f(\mathbf{p}, \tau) \ln f(\mathbf{p}, \tau) - (1 + f(\mathbf{p}, \tau)) \ln(1 + f(\mathbf{p}, \tau)) \right\} . \quad (26)$$

The dashed lines are $s = 4\epsilon/3T_{eq}$, the ideal gas form of the equilibrium entropy. To look at the actual time dependence of the generated entropy, we plotted the product of the entropy density and τ , $s\tau$, which is proportional to the total entropy in the central region in Fig. 1 and 3 (f). At LHC, the entropy no longer increases or stopped being produced at the end at $\tau = 8.75$ fm/c, whereas at RHIC, it has not yet stopped to increase at $\tau = 3.55$ fm/c when the estimated temperature falls below 200 MeV.

To check for isotropy in momentum distribution, we plotted the ratio of longitudinal to transverse pressure in Fig. 1 and 3 (d). These pressures are as defined in Sect. 2. The solid curve in each case is this ratio while the dashed curve is the ratio of a third of the energy density to the transverse pressure for comparison. The plasma starts off in an isotropic momentum configuration and becomes anisotropic due to the tendency of the plasma to free stream in the z-direction. This anisotropy attains its maximum at about 1.35 fm/c at LHC and 2.2 fm/c at RHIC. Since the plasma is approaching equilibrium, both p_L/p_T and $\epsilon/3p_T$ must approach 1.0 with increasing time. The figures show the plasma has not quite regained isotropy in momentum distribution although it

is much closer at LHC than at RHIC. Note that $p_L < \epsilon/3$ except at the start therefore less work is required for the expansion than in the case of hydrodynamic expansion when $p_L = \epsilon/3$. The consequence is the energy density drops less fast with increasing τ . Note that this does not necessarily mean that the plasma can last longer than if it underwent hydrodynamic expansion. Particle production rate must also be compared because although this does not change the energy density, it does reduce the temperature whenever the concept of a temperature makes sense. If the rate is not so rapid that it over compensates for the reduction in p_L , then indeed the plasma can last longer than that undergoing hydrodynamic expansion before phase transition takes place.

To look at the relative importance of free streaming and collisions, we plotted in Fig. 2 and 4 (a), the modified screening mass squared (solid curves) and that of free streaming when collisions have been switched off. The modified screening mass squared is

$$m_D^2(\tau) = \frac{\tau_0}{\tau} j(\tau_0/\tau) m_{D0}^2 e^{-x(\tau)} + 4\pi\alpha_s e^{-x(\tau)} \int_{\tau_0}^{\tau} \frac{d\tau'}{\theta(\tau')} \frac{\tau'}{\tau} j(\tau'/\tau) T_{eq}^2(\tau') e^{x(\tau')} \quad (27)$$

where

$$j(r) = \frac{\sin^{-1} \sqrt{1-r^2}}{\sqrt{1-r^2}} \quad (28)$$

and that of free streaming is obtained by letting $\theta \rightarrow \infty$. The latter is a decreasing function of time so free streaming increases the screening length inside the plasma since the gluon density decreases with τ^{-1} . Whereas collisions tend to shorten the screening length or increase the screening mass due to the equilibrium value is several times higher. We see that even at the beginning, collision effect is already very strong especially at LHC where $\theta_0 \sim 0.84$ when $\tau_0 \sim 0.5$ so the plasma starts very much in the mixed phase of free streaming and hydrodynamic expansion. This is less so at RHIC with $\theta_0 \sim 2.7$ when $\tau_0 \sim 0.7$ but the collision effect is still strong. In both cases, the screening mass increases first with time (more rapid increase at LHC than at RHIC) before it decreases eventually because the plasma is undergoing expansion and therefore cooling. Fig. 2 and 4 (b) show the convergence of $m_D^2(\tau)$ with the equilibrium value with increasing τ . Again, we see a better convergence at LHC than at RHIC.

Another evidence for the strong collision effects is the time dependence of the collision time $\theta(\tau)$ plotted in Fig. 2 and 4 (c) (These curves are relatively rough but because of the time required for the computations, we do not attempt to get smoother curves. In any case, how θ is evolving with time is clear.). One expects free streaming to drive the system further out of equilibrium and hence increases θ . Fig. (c)'s show quite the opposite behaviour of a clear initial drop in θ in each case. A much steeper drop at RHIC than at LHC is seen. These initial drops are followed by relatively slow increase with respect to τ . These behaviours are essential for the plasma to be able to reach equilibrium i.e. they allow τ to catch up with θ and overtake it. This overtaking of θ by τ is much more dramatic at RHIC since θ_0 is about 4 times larger than τ_0 whereas

at LHC, θ_0/τ_0 is only about 1.6. The final slow increase in θ is expected from previous calculations of relaxation time [37, 38]. They found in general when the system is near equilibrium a dependence $\tau_{relax} \sim 1/T$ on the temperature which means a time dependence of $\tau_{relax} \sim \tau^{1/3}$. In our case, we can parametrize the rate $R(\tau)$ near full equilibrium by

$$R(\tau) \approx (1-l)cT^4 = (1-l)c'a_1T^4 \quad (29)$$

where c and c' are some constants. Using Eq. (24), we get

$$\Delta n = n_{eq} - n = a_1 T^3 (l^{3/4} - l). \quad (30)$$

From the above two equations, one obtains the near equilibrium collision time $\theta_{l \rightarrow 1}(\tau)$

$$\theta_{l \rightarrow 1}(\tau) = \frac{l^{3/4}}{c'T(1+l^{1/2})(1+l^{1/4})}. \quad (31)$$

We have plotted this in Fig. 2 (c) (dashed curve) using T_{est} and l_{est} but not in Fig. 4 (c) since at RHIC, the plasma is still not yet near equilibrium. The constant c' determined from the rate is roughly $c' \approx 0.16377$. One sees that the solid and dashed curve converges at large time. One could also fit a $\tau^{1/3}$ curve on the same plot (not shown for clarity) which would show θ does have the right behaviour for a equilibrated or nearly equilibrated plasma.

Although our θ has a more complicated time dependence than simple power behaviour which was heuristically assumed in previous works [7, 11, 12] to enable simple analysis, it does satisfy the generalized condition of Heiselberg and Wang [7] for equilibration at all time. Their analysis for $\theta \sim \tau^p$ showed thermalization would be achieved for $p < 1$ otherwise θ would increase faster than τ or collision would always be slower than the expansion. For general θ , this can be reworded in terms of $x(\tau)$ defined in Eq. (5) as $x \rightarrow \infty$ as $\tau \rightarrow \infty$ for thermalization, if $x \rightarrow x_{max} < \infty$ as $\tau \rightarrow \infty$, then thermalization cannot be realized.

Finally, a word must be said about elastic collisions $gg \rightarrow gg$ which have almost been left out entirely since they drop out of Eq. (9) (their only role so far is in determining the cross-section). In [7], by considering only elastic processes, θ has been determined from the collision entropy density rate

$$\frac{\partial s}{\partial \tau} \Big|_{coll} = -\sigma' \int \frac{d^3 \mathbf{p}}{(2\pi)^3} C(\mathbf{p}, \tau) \ln \left(\frac{f}{1+f} \right) \quad (32)$$

where σ' is again some numerical factor for multiplicity etc.. They found that θ had only logarithmic time dependence. Their result, which is approximately valid in the range $2\tau_0 \lesssim \tau \ll \theta$ and after being readjusted to our initial conditions, is

$$\frac{1}{\theta} \simeq 1.55 \alpha_s^2 l_0 T_0 \ln \left(\frac{3\pi\tau}{2l_0 \alpha_s \tau_0} \right) \ln \left(\frac{2\tau}{\tau_0} \right). \quad (33)$$

Using τ between $2\tau_0 \lesssim \tau \lesssim \theta/2$, we find θ varies between 4.28–3.53 fm/c from $\tau \simeq 1.40$ fm/c to $\tau \simeq 1.76$ fm/c at RHIC, which is about 2.0 times higher than our θ in the same time range. At LHC, the above time range does not exist and so Eq. (33) cannot be applied. This shows that inelastic process $gg \longleftrightarrow ggg$ seems to be more efficient for thermalization than elastic $gg \rightarrow gg$ at least at RHIC. To verify this, we have checked using Eq. (32) how important is the entropy generated by elastic scattering when compared to that by inelastic scattering both at RHIC and at LHC. The result is small. We have to conclude that in our scenario the latter is the chief driving force for thermalization which contradicts the common assumption that thermalization is mainly the role of elastic processes. This conclusion is perhaps not too surprising since we have started in a momentarily thermalized plasma with some small initial fugacities when all elastic processes are “out of action”. Our figures show that the plasma quickly reaches the point of greatest departure from equilibrium before heading back progressively. In order for elastic scatterings to play a more prominent role, there need to be some means for an explosive rise in rate before that point² has been reached. This means is, however, missing. It must be said that although our conclusion on the dominance of inelastic over elastic process is independent of the initial conditions, the degree of dominance is not. Had we started with some much larger initial fugacities, say $l_0 \sim 1$, then the initial gluon multiplication rate $R(\tau = \tau_0)$ would be greatly reduced and this will affect the dominance. This can be understood in the following way. Since one cannot perturb an equilibrated gluon plasma kinetically without doing so chemically at the same time³, any perturbation will always drive a plasma in equilibrium further off chemical than kinetic equilibrium. In our case, the perturbation is the one-dimensional expansion and it is not obvious that the plasma has been chemically perturbed unlike the perturbation in the kinetic direction. This is so because the chemical perturbation due to the expansion is too small when compared to that with which we imposed on the system by having small l_0 's. For $l_0 \sim 1$, the rate in Fig. 2 and 4 (d) will not be monotonically decreasing with increasing τ . They will instead first rise to a peak before coming back down again towards zero. A typical sign that the system is going out of equilibrium before making the return [13]. In this case, clear chemical along with kinetic equilibrium are further upset by the expansion. Numerically, this has been verified with $l_0 \sim 0.8$. In this case, the relative importance of the two types of process is reduced but inelastic remains the more important one. To summarize, it is because of the fact that chemical equilibrium is always further away than kinetic equilibrium, inelastic process will always be significant in relation to elastic process in equilibration. A small l_0 will give it a bigger advantage or increased importance than a $l_0 \sim 1$

²We can reasonably expect the elastic scattering rate maximizes at this point. This is within the time range in which we compared θ 's above.

³The reverse is, however, not true. One can see this by finding a small perturbation that will hold chemical but not kinetic equilibrium.

Acknowledgements

The author would like to thank R. Baier for clearing up delicate matters on general interference effect, U. Heinz for useful comments, S. Peigné and D. Schiff for explanation of LPM. The author acknowledges financial support from the Leverhulme Trust.

References

- [1] U. Heinz, J. Letessier, J. Rafelski, J. Sollfrank and A. Tounsi, Proceedings of the 28th Rencontres de Moriond: QCD and High Energy Hadronic Interactions, Les Arcs, France, 20-27 March 1993, P.613, 621; Phys. Rev. Lett. 70 (1993) 3530.
- [2] K. Geiger and B. Müller, Nucl. Phys. B 369 (1991) 600.
- [3] K. Geiger, Phys. Rev. D 46 (1992) 4965, 4986.
- [4] T.S. Biró, E. van Doorn, B. Müller, M.H. Thomas and X.N. Wang, Phys. Rev. C 48 (1993) 1275.
- [5] P. Lévai, B. Müller and X.N. Wang, Phys. Rev. C 51 (1995) 3326.
- [6] X.N. Wang, Nucl. Phys. A 590 (1995) 47.
- [7] H. Heiselberg and X.N. Wang, Phys. Rev. C 53 (1996) 1892.
- [8] E.V. Shuryak and L. Xiong, Phys. Rev. C 49 (1994) 2203.
- [9] T. Altherr and D. Seiberg, Phys. Lett. B 313 (1993) 149; Phys. Rev. C 49 (1994) 1684.
- [10] P. Danielewicz and M. Gyulassy, Phys. Rev. D 31 (1985) 53.
- [11] G. Baym, Phys. Lett. B 138 (1984) 18.
- [12] S. Gavin, Nucl. Phys. B 351 (1991) 561.
- [13] S.M.H. Wong, Thermal and Chemical Equilibration in Relativistic Heavy Ion Collisions, preprint LPTHE-Orsay 96/26, BI-TP 96/18.
- [14] M. Gyulassy and X.N. Wang, Phys. Rev. D 44 (1991) 3501.
- [15] M. Gyulassy, M. Plümer, M. Thoma and X.N. Wang, Nucl. Phys. A 538 (1992) 37c.
- [16] M. Gyulassy and X.N. Wang, Nucl. Phys. A 544 (1992) 559c.
- [17] J. Winter, J. de Phys. 45 (1984) C6-53.

- [18] U. Heinz, Phys. Rev. Lett. 51 (1983) 351.
- [19] H.Th. Elze, M. Gyulassy and D. Vasak, Nucl. Phys. B 276 (1986) 706; Phys. Lett. B 177 (1986) 402.
- [20] H.Th. Elze and U. Heinz, Phys. Rep. 183 (1989) 81.
- [21] H.Th. Elze, Z. Phys. C 47 (1990) 647.
- [22] H. Weigert and U. Heinz, Z. Phys. C 50 (1991) 195.
- [23] U. Heinz, Proceedings of the Banff/CAP Workshop on Thermal Field Theories, F.C. Khanna et al., eds., World Scientific 1994, p.428.
- [24] J.D. Bjorken, Phys. Rev. D 27 (1983) 140.
- [25] T. Matsui, L.D. McLerran and B. Svetitsky, Phys. Rev. D 34 (1986) 783, 2047.
- [26] G. Bertsch and J.F. Gunion, Phys. Rev. D 25 (1982) 746.
- [27] T.S. Biró, B. Müller and X.N. Wang, Phys. Lett. B 283 (1992) 171.
- [28] K.J. Eskola, B. Müller and X.N. Wang, preprint HU-TFT-95-47, DUKE-TH-95-96, LBL-37642, hep-ph/9509285.
- [29] M. Gyulassy and X.N. Wang, Nucl. Phys. B 420 (1994) 583.
- [30] M. Gyulassy, M. Plümer and X.N. Wang, Phys. Rev. D 51 (1995) 3436.
- [31] R. Baier, Yu.L. Dokshitzer, S. Peigné and D. Schiff, Phys. Lett. B 345 (1995) 277.
- [32] Z. Kunszt and W.J. Stirling, Phys. Rev. D 37 (1988) 2439.
- [33] S.J. Parke and T.R. Taylor, Phys. Rev. Lett. 56 (1986) 2459.
- [34] K.J. Eskola, preprint HU-TFT-95-17, hep-ph/9503254.
- [35] G.P. Lepage, J. Comp. Phys. 27 (1978) 192.
- [36] S. de Groot, W.A. van Leuwen, and C.G. van Weert, Relativistic Kinetic Theory, North-Holland, Amsterdam (1980).
- [37] G. Baym, H. Monien, C.J. Pethick and D.G. Ravenhall, Phys. Rev. Lett. 64 (1990) 1867.
- [38] H. Heiselberg, G. Baym, C.J. Pethick and J. Popp, Nucl. Phys. A 544 (1992) 569c.

Figure Captions

Fig. 1 Results of the evolution of a gluon plasma towards equilibrium at LHC energies. The figures are (a) energy density ϵ , (b) number density n (solid curve), (c) estimated temperature T_{est} (solid curve) and fugacity l_{est} (dot-dashed curve), (d) the ratio of longitudinal to transverse pressure p_L/p_T (solid curve) and that of a third of the energy density to the transverse pressure $\epsilon/3p_T$ (dashed curve), (e) entropy density s , (f) the product of entropy density and time $s\tau$. The dashed curves in (b), in (c) and in (e) are the equilibrium number density, temperature and the ideal gas entropy $s = 4\epsilon/3T_{eq}$ associated with f_{eq} respectively.

Fig. 2 Results of the evolution of a gluon plasma towards equilibrium at LHC energies. The figures are (a) the modified screening mass squared m_D^2 (solid curve) compared with the free streaming case (dashed curve), (b) m_D^2 (solid curve) together with that in equilibrium (dashed curve), (c) collision time θ and (d) the rate R for $gg \longleftrightarrow ggg$. In this case only (not in Fig. 4), $\theta_{l \rightarrow 1}$ is also shown in (c) (dashed curve).

Fig. 3 Results of the evolution of a gluon plasma towards equilibrium at RHIC energies. The figures and curves are organized in the same way as those in Fig. 1.

Fig. 4 Results of the evolution of a gluon plasma towards equilibrium at RHIC energies. The figures and curves are organized in the same way as those in Fig. 2.

Table 1

Initial Conditions		
	<i>RHIC</i>	<i>LHC</i>
τ_0 (fm/c)	0.7	0.5
ϵ_0 (GeV/fm ³)	3.2	40.0
n_0 (fm ⁻³)	2.15	18.0
T_0 (GeV)	0.50	0.74
l_0	0.08	0.21
θ_0 (fm/c)	2.69	0.84

TABLE 1. Initial conditions for the evolution at RHIC and at LHC

FIG. 1, LHC

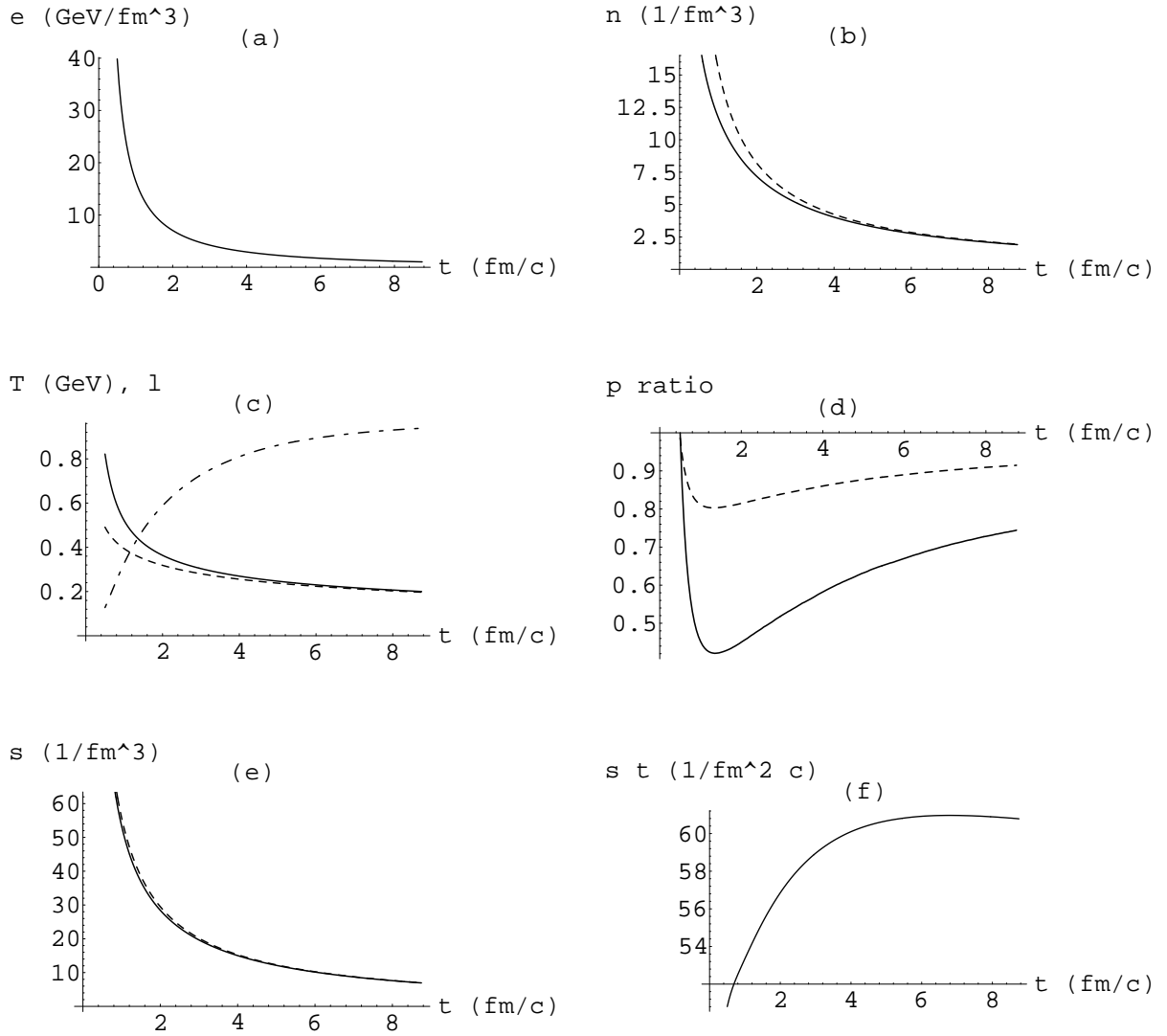


FIG. 2, LHC

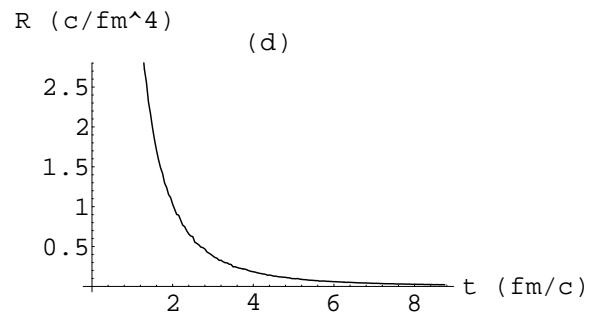
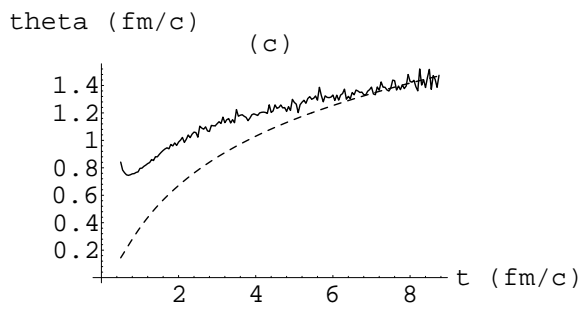
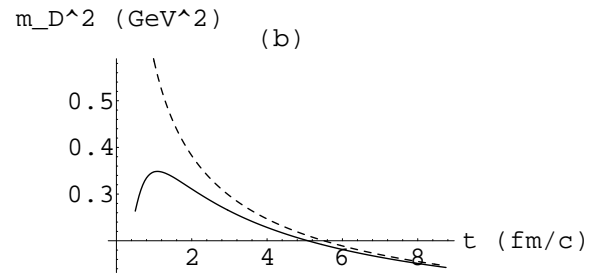
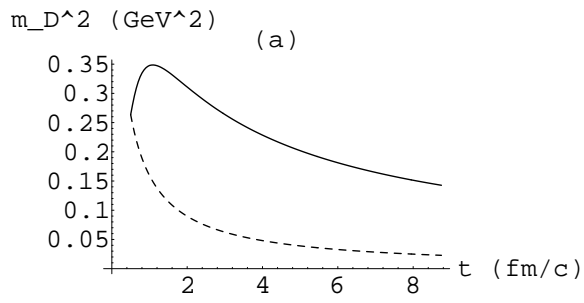


FIG. 3, RHIC

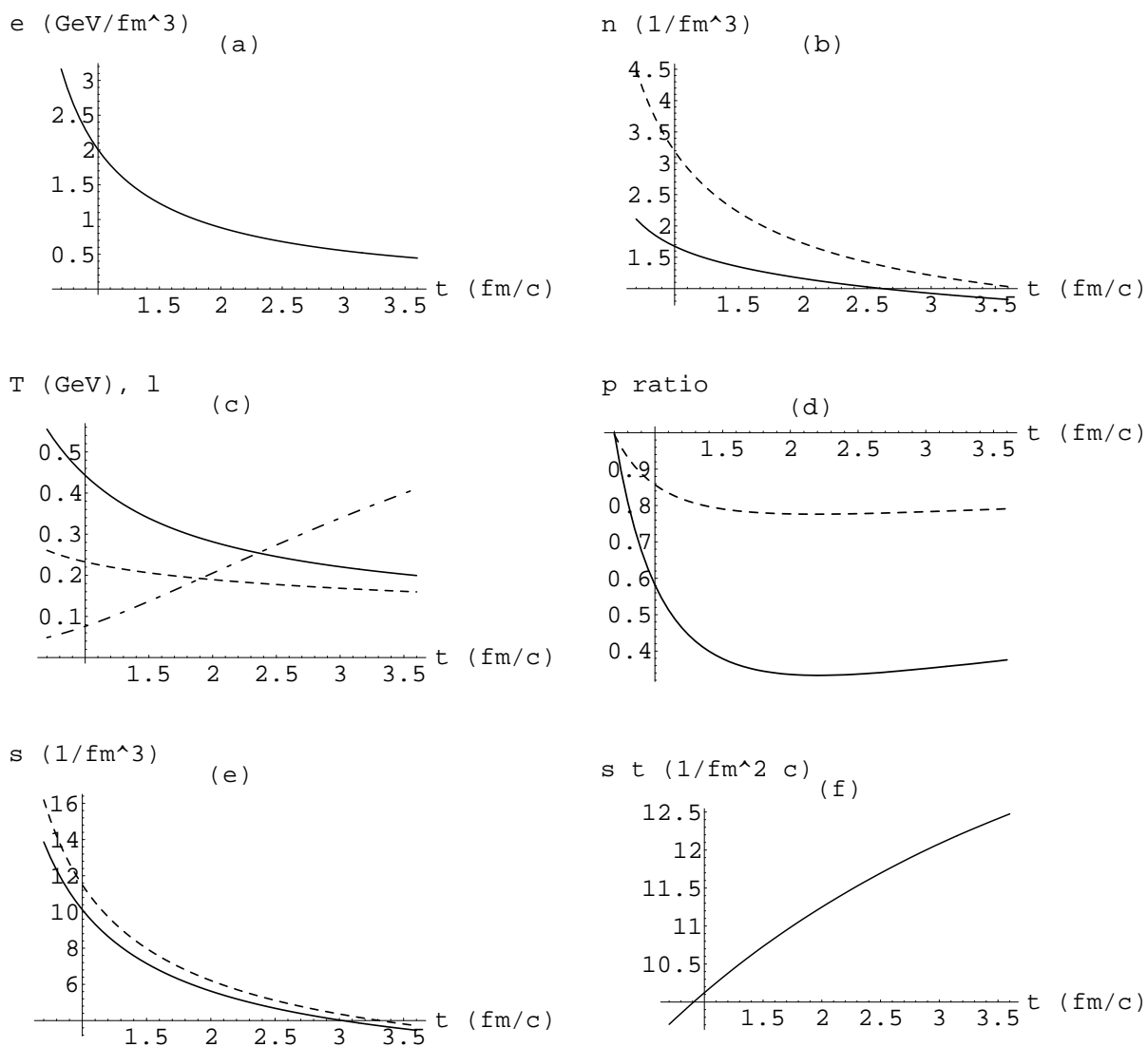


FIG. 4, RHIC

